

Near- and Mid-IR Gas-Phase Absorption Spectra of $\text{H}_2@C_{60}^+-\text{He}$

Dmitry V. Strelnikov,^{*,†} Juraj Jašík,[‡] Dieter Gerlich,[¶] Michihisa Murata,[§]
Yasujiro Murata,[§] Koichi Komatsu,[§] and Jana Roithová[‡]

[†]*Karlsruhe Institute of Technology (KIT), Division of Physical Chemistry of Microscopic
Systems, Karlsruhe, Germany*

[‡]*Department of Organic Chemistry, Faculty of Science, Charles University in Prague,
12843 Prague 2, Czech Republic*

[¶]*Department of Physics, University of Technology, 09107 Chemnitz, Germany*

[§]*Institute for Chemical Research, Kyoto University, Kyoto 611-0011, Japan*

E-mail: dmitry.strelnikov@kit.edu

Abstract

Near- and mid-IR absorption spectra of endohedral $\text{H}_2@\text{C}_{60}^+$ have been measured using He-tagging. The samples have been prepared using a 'molecular surgery' synthetic approach and were ionized and spectroscopically characterized in the gas phase. In contrast to neutral C_{60} and $\text{H}_2@\text{C}_{60}$, the corresponding He-tagged cationic species show distinct spectral differences. Shifts and line splittings in the near- and mid-IR regions indicate the influence of the caged hydrogen molecule on both the electronic ground and excited states. Possible relevance to astronomy is discussed.

Introduction

Endohedral $\text{H}_2@\text{C}_{60}$ can be synthesized in macroscopic quantities using a 'molecular surgery' approach.¹ This has already led to numerous investigations of $\text{H}_2@\text{C}_{60}$, using methods such as NMR^{2,3} or IR absorption spectroscopy.^{4,5} The H_2 inside C_{60} has enough space to behave like an almost free gas-phase molecule; however, confinement leads to observable coupling of its' rotational, vibrational and translational degrees of freedom.⁴ Recently, five of the many diffuse interstellar bands (DIBs)⁶ have been assigned to C_{60}^+ using He-tagging spectroscopy in the Basel cryogenic ion trap.⁷ This observation together with the fact that hydrogen is the most abundant element in the Universe, raises the questions of whether endohedral $\text{H}_2@\text{C}_{60}$ might be formed in Space as well and under which conditions.⁸ In contrast to the exohedral van der Waals complexes, endohedral $\text{H}_2@\text{C}_{60}^+$ can survive under ionizing conditions and higher temperatures, possibly present in some regions of Space. This stability of $\text{H}_2@\text{C}_{60}^+$ is demonstrated by the fact that this ion can be observed in electron ionization (EI) mass spectra of sublimed $\text{H}_2@\text{C}_{60}$. In order to find out whether $\text{H}_2@\text{C}_{60}^+$ is present in Space and provide guidance for astronomy, we investigated optical spectroscopic signatures of $\text{H}_2@\text{C}_{60}^+$ in the near IR range.

Experimental Methods

The experiments have been performed using the cryogenic wire quadrupole ion trap of the Prague instrument ISORI (Infrared Spectroscopy of Reaction Intermediates), described in detail in Jašík et al.^{9,10,11}. Many details concerning the production and cooling of fullerene ions and tagging them with helium atoms can be found elsewhere.^{12,13} Briefly, ions have been produced in a Finnigan Solids Probe EI-source with 65 eV electrons. Experiments have been performed with three samples, (i) 10 mg of 100% H₂@C₆₀, (ii) 10 mg of 80% H₂@C₆₀/20% C₆₀ and (iii) C₆₀ (99,5% purity). The endohedral probes have been synthesized using a ‘molecular surgery’ approach.¹ The C₆₀ sample was obtained from SES Research. Ions, emerging from the source, are mass-selected by a quadrupole mass filter and transferred via a quadrupole bender and an octopole to the cryogenic quadrupole ion trap. The temperature of the cold head has been 3.7 K. The mass-selected ions were trapped and relaxed by collisions with helium buffer gas. A part of the ions formed complexes with helium atoms. The trapped ions were probed by IR photons from an OPO system (LaserVision) pumped by a Nd:YAG laser (Surelite EX from Continuum, 10 Hz repetition rate, 6ns pulse width). Using an injection seeder the line width of the OPO is smaller than 1.5 cm⁻¹. The wavelength is measured using a high-precision wavelength meter (HighFines WS6-200). For the near-IR electronic transitions, a Sunlite EX OPO tunable System (Continuum) is used, pumped with a seeded PL 9010 (line width < 0.1 cm⁻¹). Absorption of photons was monitored by counting the number of helium complexes via a second quadrupole filter followed by an ion detector. If a complex absorbs a photon the helium is eliminated. In order to correct for any background the light beam is blocked every other second with a mechanical shutter, resulting in numbers of unperturbed ions, N_0 , while $N(\nu)$ is the number of complexes remaining after irradiation at frequency ν . For the IR measurements $N(\nu)$ was obtained from 10 Laser pulses during one second, followed by the one second N_0 accumulation. For the near-IR measurements the number of the laser pulses was reduced to one. The laser pulse energy have been changing in the 0.017-0.08 mJ range for the IR measurements and in the 0.16-0.83 mJ range for the

near-IR measurements. The laser beam diameters were 2 mm and 1 mm for the IR and near-IR measurements correspondingly. Laser scan velocities were $0.2 \text{ cm}^{-1}/\text{s}$ for the IR and $0.03 \text{ nm}/\text{s}$ for the near-IR.

We present the spectra either as attenuation spectra, plotting $1 - N(\nu)/N_0$, or we correct in first order for non-linear attenuation by calculating relative cross section using the equation: $\sigma = -\Phi^{-1} \ln(N(\nu)/N_0)$, where Φ is number of photons per cm^2 the ions have been exposed to.

Raman measurements have been performed in Karlsruhe on powder samples of neutral $\text{H}_2@C_{60}$ and C_{60} using a Raman spectrometer Kaiser Optics RXN1 (785 nm excitation, 5 cm^{-1} spectral resolution).

Results and Discussion

Vibrational spectroscopy.

Fig. 1 compares Raman spectra of 80% $\text{H}_2@C_{60}$ (red) with those from C_{60} bulk samples. A careful inspection reveals that the hydrogen inside the C_{60} does not influence the Raman spectrum. The line positions agree within 0.4 cm^{-1} . Since Raman scattering probes the vibrational levels in the electronic ground state, the state of the neutral endohedral C_{60} is the same as that of the empty C_{60} . Some weak interference in the $\text{H}_2@C_{60}$ spectrum is caused by the luminescence of traces of impurities. (The interference is an instrumental artifact. It could be clearly observed when measuring continuous spectra. Probably, it is generated in the optical fiber of the Raman probe.)

Fig. 2 compares our gas-phase spectra for $\text{H}_2@C_{60}^+-\text{He}$ with $C_{60}^+-\text{He}$ from Gerlich et al.¹² and with C_{60}^+ recorded in a cryogenic Ne-matrix.¹⁴ The two gas-phase spectra differ in the bands' shifts and splittings. These differences reflect the influence of H_2 on the ground state of C_{60}^+ . Contrary to the neutral systems (see above), the cations apparently interact more strongly with the H_2 molecule inside. The C_{60}^+ cation has a D_{5d} ground state symmetry,¹⁴

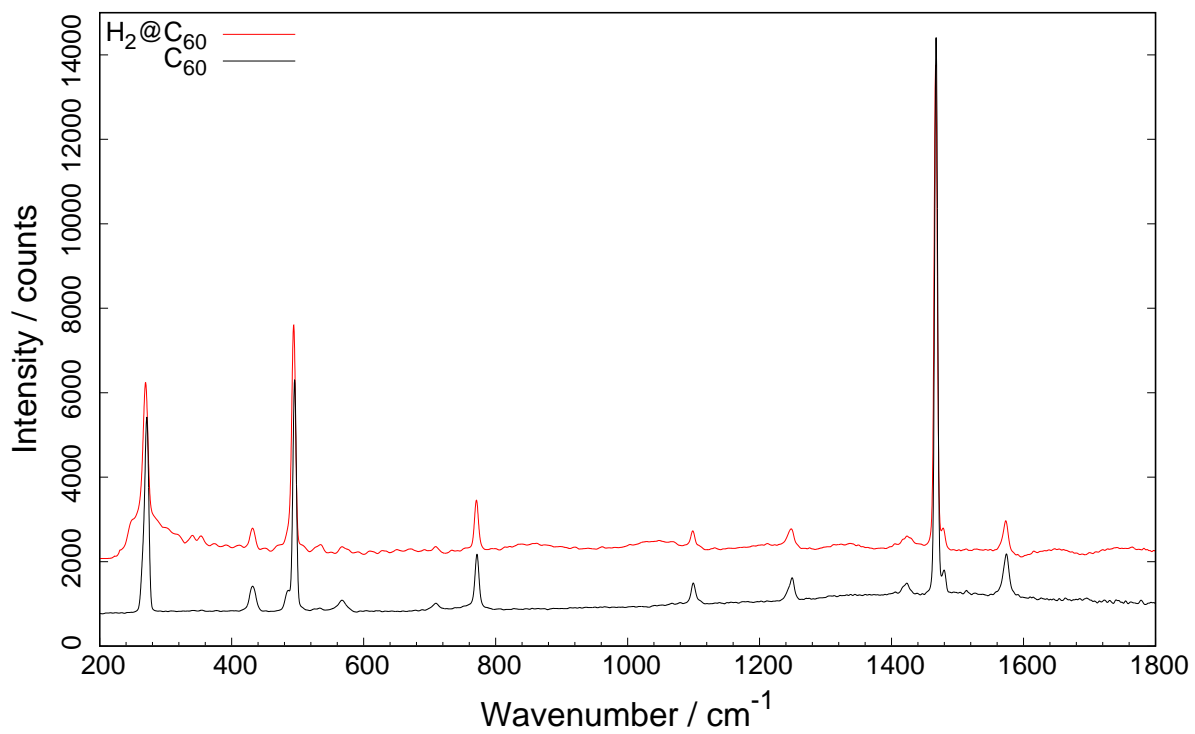


Figure 1: Raman spectra of the bulk H₂@C₆₀ (red) and C₆₀ (black) samples. CW laser excitation at 785 nm, 50 mW.

therefore, not all directions for translational motion of H_2 inside the cage are equivalent. H_2 can move further from the fullerene center of gravity along the C_5 symmetry axis. In addition, a delocalized positive charge on a fullerene cage enhances the van der Waals interaction with H_2 .

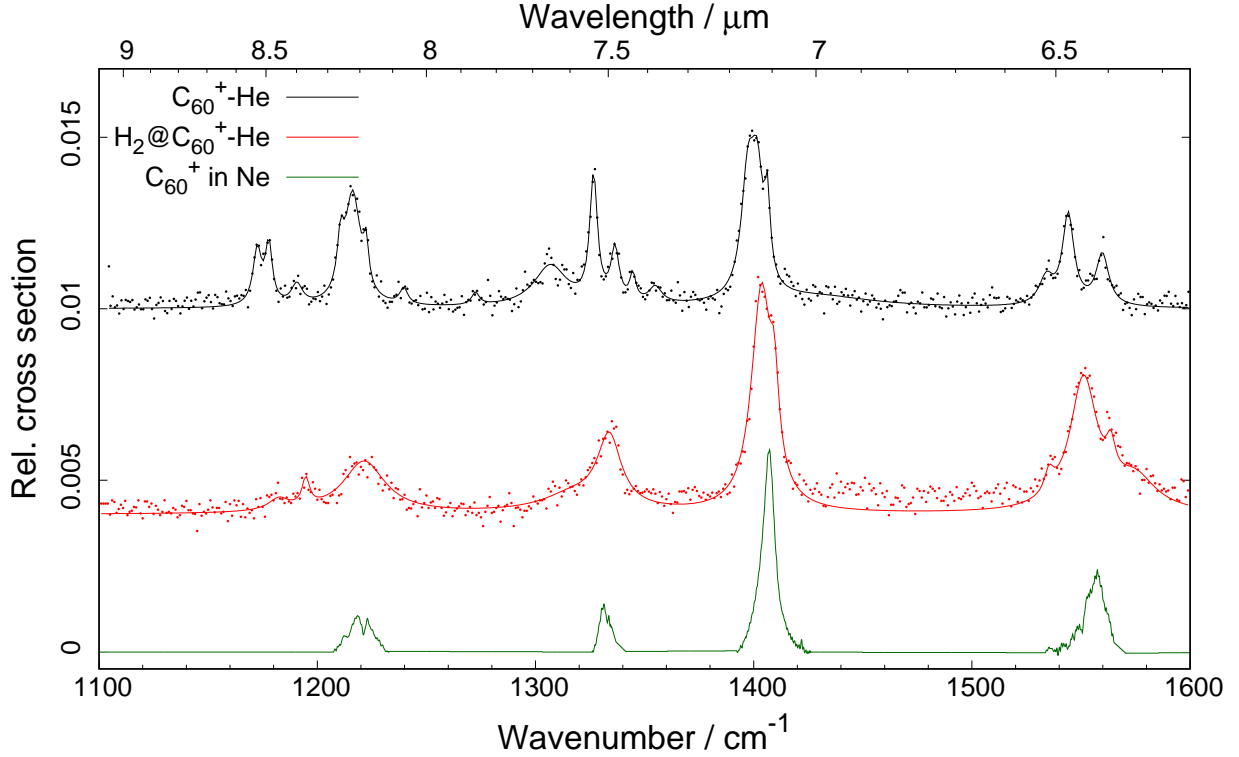


Figure 2: IR absorption spectra of $\text{H}_2@\text{C}_{60}^+-\text{He}$ (middle panel) compared with data for $\text{C}_{60}^+-\text{He}$ ¹² and for C_{60}^+ in Ne matrix.¹⁴ The experimental data are fitted with Lorentzians. Intensities of the $\text{H}_2@\text{C}_{60}^+-\text{He}$ and $\text{C}_{60}^+-\text{He}$ spectra are scaled down for a better comparison with C_{60}^+ in Ne.

The structure of the IR absorptions in the helium tagged fullerene ions may originate from the interaction with the attached He atom or be caused by vibrational coupling of C-C modes, the details are discussed elsewhere.¹²

The splittings of IR bands differ for $\text{H}_2@\text{C}_{60}^+-\text{He}$ and $\text{C}_{60}^+-\text{He}$. The $\text{H}_2@\text{C}_{60}^+-\text{He}$ has a reduced splitting in comparison to the empty $\text{C}_{60}^+-\text{He}$. In addition, the band at 1170 cm^{-1} is either very weak or absent for $\text{H}_2@\text{C}_{60}^+-\text{He}$. These effects are apparently induced by the distortion from H_2 , but the theoretical calculations do not offer a reasonable qualitative

explanation of this effect. Surprisingly, the IR spectrum of $\text{H}_2@\text{C}_{60}^+-\text{He}$ resembles more the IR spectrum of C_{60}^+ in neon matrix than that of $\text{C}_{60}^+-\text{He}$ in the gas phase. A qualitative outcome of this measurement is the following: the more perturbation C_{60}^+ experiences, the larger blue shift and the smaller band splitting are observed. At present, we are not able to rationalize this by the DFT calculations (see Supporting information). The Lorentzian fit parameters of the experimental data: the band positions, relative heights and FWHMs are compared in Table 1.

Table 1: Parameters of the Lorentzian fits (see Fig.2): positions of the IR absorptions (cm^{-1}), relative heights (x1000) and FWHM (cm^{-1}).

$\text{C}_{60}^+-\text{He}$ ^a			$\text{H}_2@\text{C}_{60}^+-\text{He}$			C_{60}^+ in Ne ^b		
ν	rel. height	FWHM	ν	rel. height	FWHM	ν	rel. height	FWHM
1172.5	0.6	4.8						
1177.8	0.7	3.9	1182.4	0.3	11.3			
1190.7	0.2	6.1	1194.7	0.8	4.1			
1210.7	0.5	3.6				1212.5	0.3	4.0
1216.3	1.4	8.7				1218.1	1.0	4.6
1222.4	0.5	2.8	1221.4	1.5	23.6	1223.7	0.8	4.0
1239.6	0.2	4.4						
1272.5	0.1	4.2						
1306.8	0.5	18.4	1317.4	0.5	35.5			
1326.6	1.8	4.2	1333.8	2.1	13.3	1331.1	1.2	3.2
1336.4	0.7	4.5				1333.6	0.5	1.2
1344.6	0.3	3.2				1335.15	0.5	1.9
1354.9	0.2	7.2						
1397.3	1.7	7.2	1403.5	6.4	11.0	1407.12	5.5	7.4
1401.6	1.6	6.8	1409.4	2.3	4.7			
1406.3	1.1	3.0						
1428.9	0.1	66.3						
1534.1	0.4	7.9	1535.4	0.6	5.2			
1544.1	1.4	6.4	1551.2	3.8	15.1	1557.6	2.2	9.2
1559.8	0.8	7.0	1563.6	0.9	5.0			
			1574.8	0.9	23.1			

^a Data from Gerlich et al.¹²; ^b Data from Kern et al.¹⁴.

Electronic spectroscopy.

The geometry of a linear quadrupole trap together with high laser fluence in our experimental setup allows relatively fast acquisition of overview spectra: the 860 – 970 nm region have been scanned in about one hour. Comparison of our data with Campbell et al.⁷, Campbell and Maier¹⁵ reveals minor differences in band positions (about 0.3 Å) but pronounced deviations in band widths and intensities (see Figs. S1,S2 in Supporting Information). These deviations originate from the non-linearities, caused by a high laser power in our measurements. The high laser power leads to the saturation of strong absorption lines, but allows to see weak absorptions. Although the attenuation for many saturated bands is about 0.8 (see below), these bands show definitively a saturation effect. The experimental geometry of the ISORI setup is such, that one has a complete overlap of the laser beam and the trapped ions. Currently, the saturation effects are not completely understood and require further dedicated experiments. Despite the deviations, the fast overview scan allows to obtain reliable absorption wavelengths. An estimate of the absorption intensities is more difficult. This can be seen from the fact that we observed more spectral bands of C_{60}^+ -He than previously reported.^{7,15} Some of the narrow lines have been not resolved, because of the 0.25 nm step wavelength sampling. For a better resolution one would need to scan slowly with a denser sampling. The electronic spectra of C_{60}^+ -He and $H_2@C_{60}^+$ -He show pronounced differences in band positions as well as in the band structures at higher energies (Fig. 3). Hence, importantly the near-IR absorption spectra of C_{60}^+ and $H_2@C_{60}^+$ can be clearly distinguished. We fitted the spectra with Lorentzian functions and present the obtained fit parameters in Table 2. Because of the limited time for the measurements, we did not obtain absolute cross sections of the observed $H_2@C_{60}^+$ -He absorption bands, which require power dependence measurements. However, we used identical experimental settings for both measurements: C_{60}^+ -He and $H_2@C_{60}^+$ -He. Thus the measured absorption intensities for both systems are comparable (Fig. 3), and therefore the absolute absorption cross sections should be also similar. For a direct comparison with astronomical data, one should consider a possible influence of an

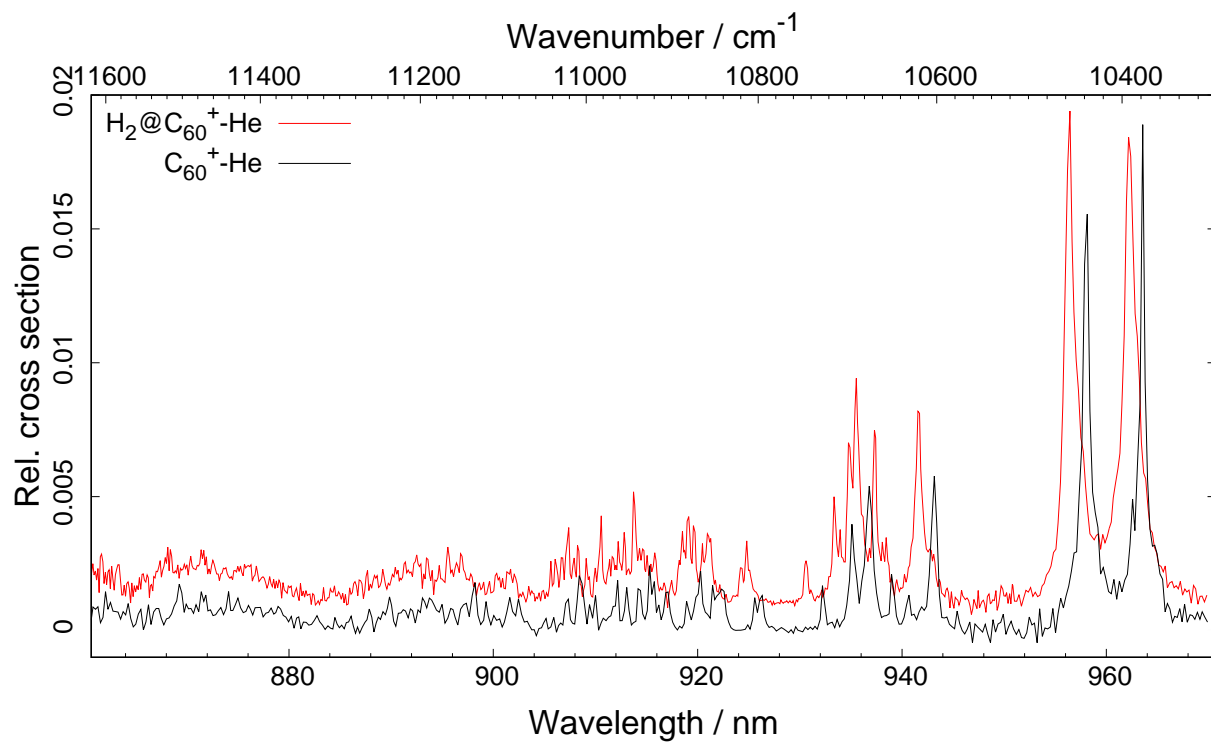


Figure 3: An overview near-IR absorption spectra of C₆₀⁺ vs. H₂@C₆₀⁺. Both spectra are measured with the same settings. The relative line intensities of each spectrum may deviate from the unsaturated one-photon absorption spectra due to a high laser fluence.

attached He atom on the absorption wavelengths. As in the case of C_{60}^+ , we expect for an untagged $H_2@C_{60}^+$ a $\sim 0.7 \text{ \AA}$ blue shift¹⁶ of the near-IR absorption wavelengths. In addition, the presented here vacuum wavelengths should be converted to the air values. Inspection of the present DIBs catalogues^{17,18} reveals no absorption bands, corresponding to $H_2@C_{60}^+$. The upper limit estimation for the presence of $H_2@C_{60}^+$ in the interstellar medium depends on the signal to noise ratio of the astronomical data. There is a complication arising from the atmospheric water absorption lines in the near-IR region. Using the astronomical data^{19,20} we estimated the upper limit for the $H_2@C_{60}^+$ to C_{60}^+ ratio to be ~ 0.1 .

Table 2: Parameters of the Lorentzian fits (see Fig.3): positions of the NIR absorptions (λ / nm), relative heights and FWHM (nm). Wavelengths are given in vacuum values.

$H_2@C_{60}^+-\text{He}$			$C_{60}^+-\text{He}$		
λ	rel. height	FWHM	λ	rel. height	FWHM
962.33	0.0165	1.64	963.57	0.0170	0.68
956.42	0.0171	1.27	958.04	0.0145	1.01
942.89	0.0013	0.93			
941.61	0.0069	0.76	943.14	0.0055	0.68
938.37	0.0016	0.80	940.63	0.0010	0.39
937.33	0.0061	0.41	939.01	0.0014	0.54
935.55	0.0073	0.81	936.80	0.0049	0.85
934.80	0.0048	0.33			
933.38	0.0035	0.39	935.14	0.0032	0.63
930.60	0.0016	0.38	932.25	0.0016	0.27
924.85	0.0019	0.56	926.24	0.0018	0.23
921.07	0.0025	0.79	922.43	0.0015	0.45
919.63	0.0023	0.29	921.48	0.0013	0.31
919.08	0.0031	0.41	920.29	0.0019	0.40
918.49	0.0022	0.34	919.79	0.0007	0.49
915.83	0.0017	0.43	916.98	0.0014	0.52
913.77	0.0041	0.34	915.31	0.0020	0.31
912.83	0.0022	0.34	914.29	0.0016	0.40
910.53	0.0031	0.27	912.16	0.0015	0.28
907.31	0.0028	0.33	908.50	0.0020	0.59

Fig.4 shows a section from Fig. 3 as attenuation. For better comparison, the $H_2@C_{60}^+-\text{He}$ spectrum has been blue-shifted by about 1.5 nm with respect to the $C_{60}^+-\text{He}$ spectrum.

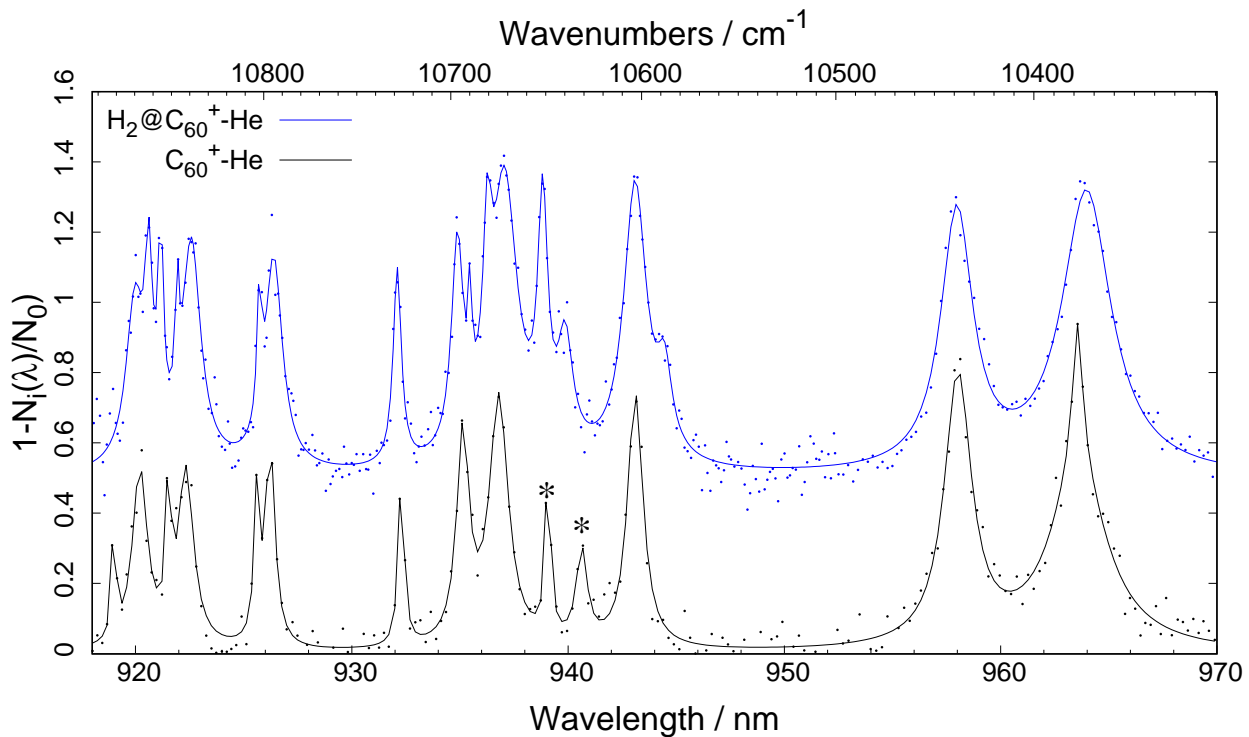


Figure 4: Near-IR photo-depletion spectra of C_{60}^+ vs. $H_2@C_{60}^+$. $N(\lambda)$ is the number of survived He-complexes after the laser irradiation, N_0 is the number of the He-complexes in the absence of laser. The $H_2@C_{60}^+$ spectrum is shifted by 1.5 nm to the longer wavelengths for an easier comparison of both spectra. ‘*’ indicate newly observed weak absorption bands of C_{60}^+ .

Detailed inspection reveals that some of the lines in the $\text{H}_2@C_{60}^+$ -He spectrum exhibit some splitting. Apparently, H_2 perturbs the excited state of C_{60}^+ . This is, however, not surprising, since the ground state is also influenced by the presence of H_2 inside the cage. So far there is no theoretical work, properly describing and explaining the vibronic transitions of C_{60}^+ in the ${}^2E_{1g}$ state. With a hydrogen molecule inside the cage it is an even more challenging system for a theoretical treatment than C_{60}^+ . TDDFT was done for several different orientations of H_2 . The theory predicts the blue shifts up to 2.5 nm and also the splitting for some of the H_2 positions (see Supporting Information). Line shifts in the electronic spectrum, introduced by H_2 inside a fullerene are much larger, than those, induced by adsorption of Ne, Ar, N_2 , H_2 , D_2 outside the C_{60}^+ .²¹ The external molecule/atom adsorption on C_{60}^+ molecules mostly leads to red shifts in the near-IR spectra.²¹ Conversely, we observe a considerable blue shift in the spectrum of the endohedral $\text{H}_2@C_{60}^+$ ion.

Conclusion

Gas-phase mid-IR and near-IR measurements show distinct spectral differences between $\text{H}_2@C_{60}^+$ and C_{60}^+ . The correct quantitative description of the observed differences in the absorptions requires dedicated theoretical modeling. There are no known DIBs at the absorption positions of $\text{H}_2@C_{60}^+$. The estimated upper limit of the interstellar $\text{H}_2@C_{60}^+/C_{60}^+$ ratio is ~ 0.1 .

Acknowledgement

The project was funded by the European Research Council (ERC CoG No. 682275) and the Deutsche Forschungsgemeinschaft (KA 972/10-1). We also acknowledge support by KIT and Land Baden-Württemberg.

References

- (1) Komatsu, K.; Murata, M.; Murata, Y. Encapsulation of Molecular Hydrogen in Fullerene C60 by Organic Synthesis. *Science* **2005**, *307*, 238–240
- (2) Carravetta, M.; Johannessen, O. G.; Levitt, M. H.; Heinmaa, I.; Stern, R.; Samoson, A.; Horsewill, A. J.; Murata, Y.; Komatsu, K. Cryogenic NMR Spectroscopy of Endohedral Hydrogen-Fullerene Complexes. *J. Chem. Phys.* **2006**, *124*, 104507
- (3) Sartori, E.; Ruzzi, M.; Turro, N. J.; Decatur, J. D.; Doetschman, D. C.; Lawler, R. G.; Buchachenko, A. L.; Murata, Y.; Komatsu, K. Nuclear Relaxation of H₂ and H₂@C₆₀ in Organic Solvents. *J. Am. Chem. Soc.* **2006**, *128*, 14752–14753, PMID: 17105254
- (4) Mamone, S.; Ge, M.; Huvonen, D.; Nagel, U.; Danquigny, A.; Cuda, F.; Grossel, M. C.; Murata, Y.; Komatsu, K.; Levitt, M. H. et al. Rotor in a Cage: Infrared Spectroscopy of an Endohedral Hydrogen-Fullerene Complex. *J. Chem. Phys.* **2009**, *130*, 081103
- (5) Rõõm, T.; Peedu, L.; Ge, M.; Huvonen, D.; Nagel, U.; Ye, S.; Xu, M.; Bačić, Z.; Mamone, S.; Levitt, M. H. et al. Infrared Spectroscopy of Small-Molecule Endofullerenes. *Philos. Trans. R. Soc., A* **2013**, *371*
- (6) Snow, T. P.; McCall, B. J. Diffuse Atomic and Molecular Clouds. *Annu. Rev. Astron. Astrophys.* **2006**, *44*, 367–414
- (7) Campbell, E. K.; Holz, M.; Maier, J. P.; Gerlich, D.; Walker, G. A. H.; Bohlender, D. Gas Phase Absorption Spectroscopy of C₆₀⁺ and C₇₀⁺ in a Cryogenic Ion Trap: Comparison with Astronomical Measurements. *Astrophys. J.* **2016**, *822*, 17
- (8) Omont, A. Interstellar fullerene compounds and diffuse interstellar bands. *Astron. Astrophys.* **2016**, *590*, A52
- (9) Jašík, J.; Žabka, J.; Roithová, J.; Gerlich, D. Infrared Spectroscopy Of Trapped Molecu-

lar Dications Below 4K. *Int. J. Mass Spectrom.* **2013**, *354-355*, 204 – 210, Detlef Schröder Memorial Issue

- (10) Jašík, J.; Gerlich, D.; Roithová, J. Two-Color Infrared Predissociation Spectroscopy of $C_6H_6^{2+}$ Isomers Using Helium Tagging. *J. Phys. Chem. A* **2015**, *119*, 2532–2542, PMID: 25402726
- (11) Jašík, J.; Navrátil, R.; Němec, I.; Roithová, J. Infrared and Visible Photodissociation Spectra of Rhodamine Ions at 3 K in the Gas Phase. *J. Phys. Chem. A* **2015**, *119*, 12648–12655, PMID: 26595323
- (12) Gerlich, D.; Jašík, J.; Strelnikov, D.; Roithová, J. IR spectroscopy of fullerene ions in a cryogenic quadrupole trap. **2018**, *Astrophys. J.*, in press
- (13) Gerlich, D.; Jašík, J.; Roithová, J. Tagging fullerene ions with helium in a cryogenic quadrupole trap. **2018**, In preparation for the special issue of the International Journal of Mass Spectrometry to honor Professor Helmut Schwarz
- (14) Kern, B.; Strelnikov, D.; Weis, P.; Böttcher, A.; Kappes, M. M. IR Absorptions of C_{60}^+ and C_{60}^- in Neon Matrixes. *J. Phys. Chem. A* **2013**, *117*, 8251–8255
- (15) Campbell, E. K.; Maier, J. P. Isomeric and Isotopic Effects on the Electronic Spectrum of C_{60}^+-He : Consequences for Astronomical Observations of C_{60}^+ . *Astrophys. J.* **2018**, *858*, 36
- (16) Campbell, E. K.; Holz, M.; Maier, J. P. C_{60}^+ in Diffuse Clouds: Laboratory and Astronomical Comparison. *Astrophys. J., Lett.* **2016**, *826*, L4
- (17) Hobbs, L. M.; York, D. G.; Snow, T. P.; Oka, T.; Thorburn, J. A.; Bishof, M.; Friedman, S. D.; McCall, B. J.; Rachford, B.; Sonnentrucker, P. et al. A Catalog of Diffuse Interstellar Bands in the Spectrum of HD 204827. *Astrophys. J.* **2008**, *680*, 1256–1270

- (18) Hamano, S.; Kobayashi, N.; Kondo, S.; Sameshima, H.; Nakanishi, K.; Ikeda, Y.; Yasui, C.; Mizumoto, M.; Matsunaga, N.; Fukue, K. et al. Near Infrared Diffuse Interstellar Bands Toward the Cygnus OB2 Association. *Astrophys. J.* **2016**, *821*, 42
- (19) Walker, G. A. H.; Bohlender, D. A.; Maier, J. P.; Campbell, E. K. Identification of More Interstellar C₆₀⁺ Bands. *Astrophys. J., Lett.* **2015**, *812*, L8
- (20) Cox, Nick L. J.; Cami, Jan.; Farhang, Amin.; Smoker, Jonathan.; Monreal-Ibero, Ana.; Lallement, Rosine.; Sarre, Peter J.; Marshall, Charlotte C. M.; Smith, Keith T.; Evans, Christopher J., et al. The ESO Diffuse Interstellar Bands Large Exploration Survey (EDIBLES) - I. Project description, survey sample, and quality assessment. *Astron. Astrophys.* **2017**, *606*, A76
- (21) Holz, M.; Campbell, E. K.; Rice, C. A.; Maier, J. P. Electronic Absorption Spectra of C₆₀+L (L=He, Ne, Ar, Kr, H₂, D₂, N₂) Complexes. *J. Mol. Spectrosc.* **2017**, *332*, 22 – 25, Molecular Spectroscopy in Traps
- (22) Rohatgi, A. WebPlotDigitizer. <https://automeris.io/WebPlotDigitizer>, Version: 4.1, E-Mail: ankitrohatgi@hotmail.com, Location: Austin, Texas, USA
- (23) TURBOMOLE V6.4 2012, a development of University of Karlsruhe and Forschungszentrum Karlsruhe GmbH, 1989-2007, TURBOMOLE GmbH, since 2007; available from <http://www.turbomole.com>

Supporting Information

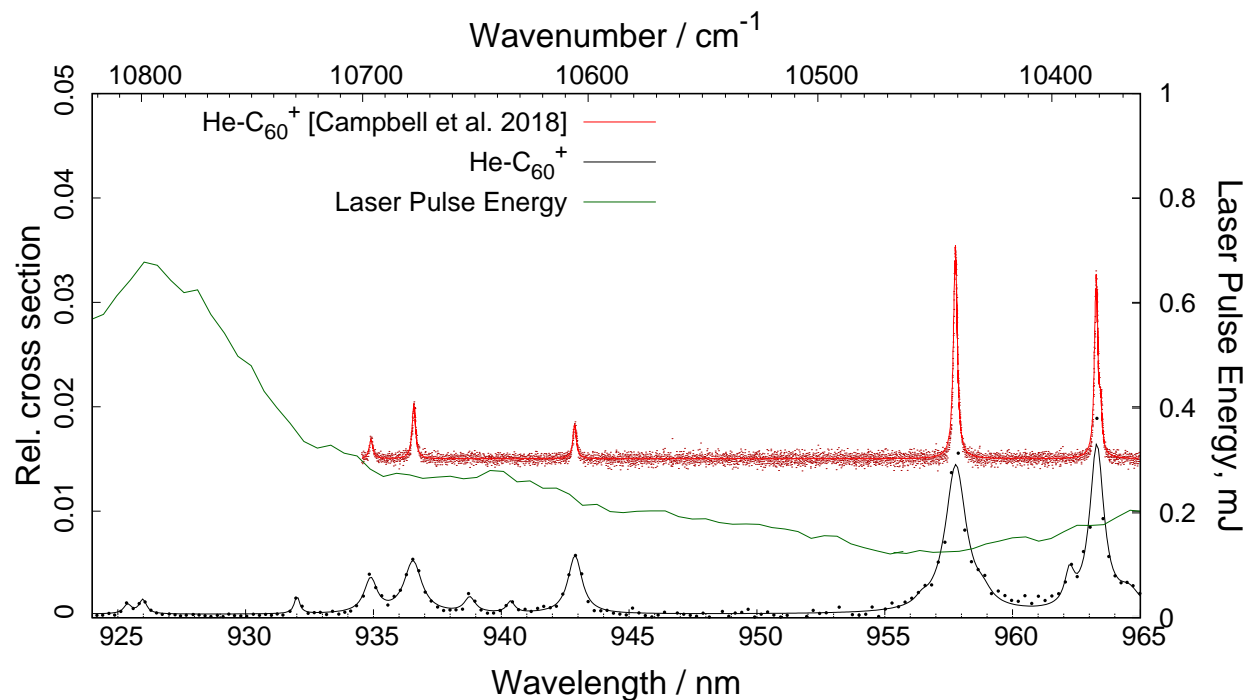


Figure S1: Comparison of our near-IR data to the Campbell and Maier¹⁵. Here the vacuum wavelengths were converted to the air wavelengths, used in Campbell and Maier¹⁵. The data points from Campbell and Maier¹⁵ have been digitized using *WebPlotDigitizer*.²²

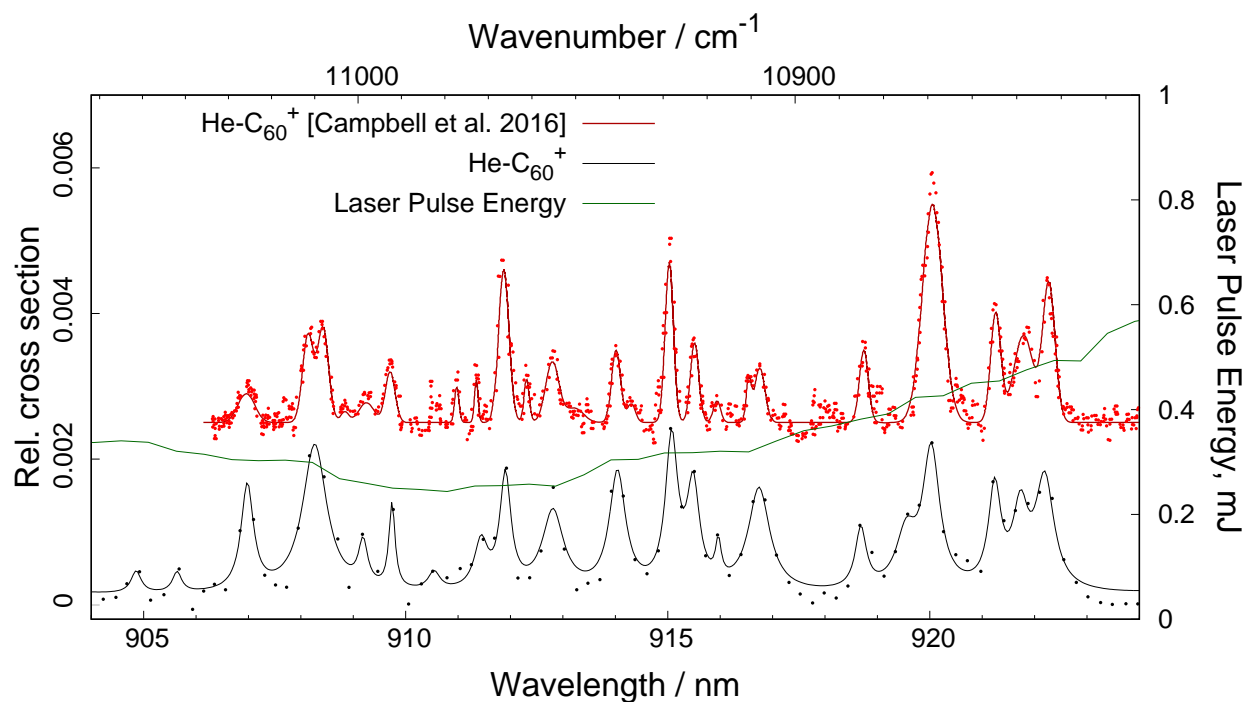


Figure S2: Comparison of our near-IR data to the Campbell et al.⁷. Here the vacuum wavelengths were converted to the air wavelengths used in Campbell et al.⁷. The data points from Campbell et al.⁷ have been digitized using *WebPlotDigitizer*.²²

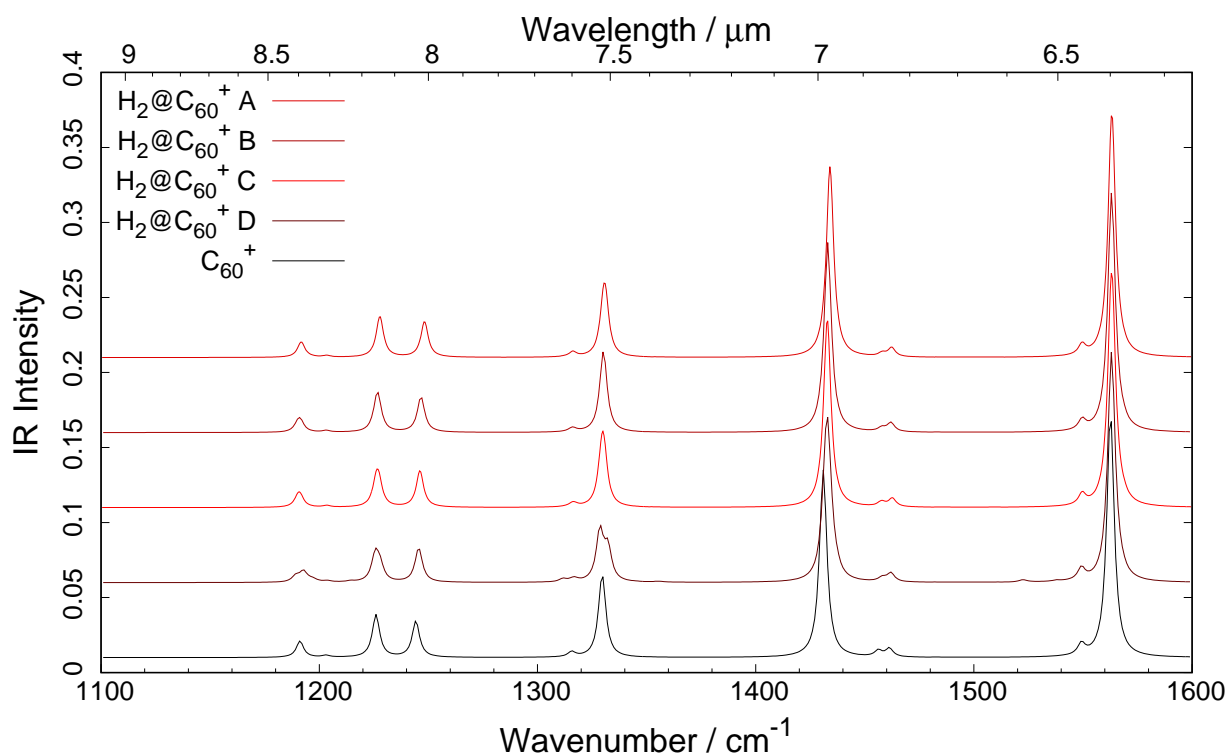


Figure S3: Calculated harmonic frequencies (RI-DFT BP86/def2-SVP, D3 dispersion correction²³) of isomers with different H₂ orientations inside C₆₀⁺. The calculated spectrum was broadened by Lorentzian functions with a 4 cm⁻¹ FWHM. The potential energy surface for H₂ inside C₆₀⁺ is very shallow, hindering a proper geometry optimization. Therefore, we took few H₂@C₆₀⁺ isomers, which are not the real ground states due to the presence of imaginary frequencies, corresponding to H₂ motion inside C₆₀⁺. Nevertheless, the applied level of theory does not predict considerable influence of H₂ on the C-C stretching (tangential) vibrational modes.

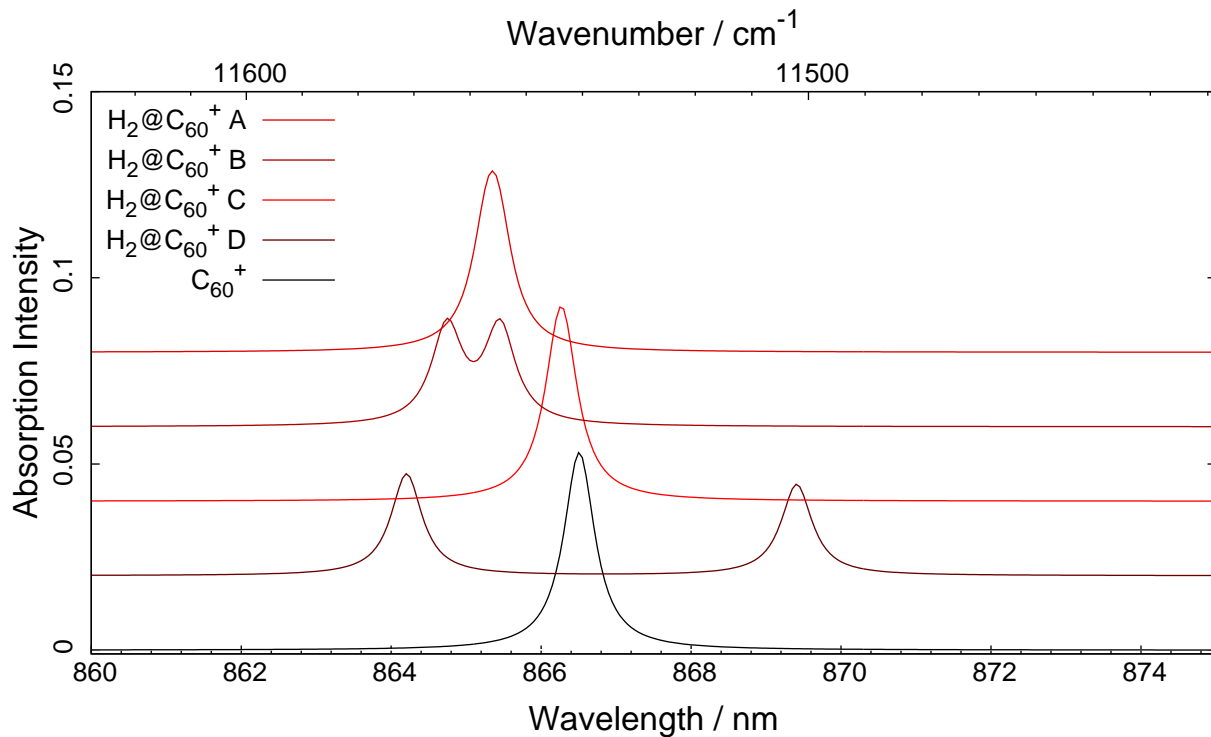


Figure S4: Calculated 0-0 vertical electronic transitions, corresponding to the $C_{60}^+ \ ^2E_{1g} \leftarrow \ ^2A_{1u}$ absorption (TDDFT BP86/def2-SVP)²³ for the same $H_2@C_{60}^+$ isomers as in Fig. S3. The calculated spectrum was broadened by Lorentzian functions with a 0.5 nm FWHM: oscillator strength \times Lorentzian function. Most of the calculated absorption wavelengths show a blue shift relative to the C_{60}^+ absorption, which is also observed in the experiment.